Hindawi Publishing Corporation
Journal of Nanomaterials
Volume 2014, Article ID 176015, 12 pages
http://dx.doi.org/10.1155/2014/176015

Research Article

Synthesis and Physicochemical Characterization of Mesoporous SiO_2 Nanoparticles

Dharani Das,[1] Yong Yang,[2] Julie S. O'Brien,[3] Dalibor Breznan,[3] Surendra Nimesh,[3] Stéphane Bernatchez,[4] Myriam Hill,[4] Abdelhamid Sayari,[2] Renaud Vincent,[3] and Prem Kumarathasan[1]

[1] *Analytical Biochemistry and Proteomics Laboratory, Environmental Health Science and Research Bureau, Healthy Environments and Consumer Safety Branch, Health Canada, Canada*
[2] *Department of Chemistry, Centre for Catalysis Research and Innovation (CCRI), University of Ottawa, Ottawa, Canada*
[3] *Inhalation Toxicology Laboratory, Environmental Health Science and Research Bureau, Healthy Environments and Consumer Safety Branch, Health Canada, Canada*
[4] *Nanotechnology Section, New Substances Assessment and Control Bureau, Healthy Environments and Consumer Safety Branch, Health Canada, Canada*

Correspondence should be addressed to Prem Kumarathasan; premkumari.kumarathasan@hc-sc.gc.ca

Received 27 December 2013; Revised 21 March 2014; Accepted 24 March 2014; Published 18 May 2014

Academic Editor: Miguel A. Correa-Duarte

There exists a knowledge gap in understanding potential toxicity of mesoporous silica nanoparticles. A critical step in assessing toxicity of these particles is to have a wide size range with different chemistries and physicochemical properties. There are several challenges when synthesizing mesoporous silica nanoparticles over a wide range of sizes including (1) nonuniform synthesis protocols using the same starting materials, (2) the low material yield in a single batch synthesis (especially for particles below 60–70 nm), and (3) morphological instability during surfactant removal process and surface modifications. In this study, we synthesized a library of mesoporous silica nanoparticles with approximate particle sizes of 25, 70, 100, 170, and 600 nm. Surfaces of the silica nanoparticles were modified with hydrophilic-CH_2–$(CH_2)_2$–COOH and relatively hydrophobic-CH_2–$(CH_2)_{10}$–COOH functional groups. All silica nanoparticles were analysed for morphology, surface functionality, surface area/pore volume, surface organic content, and dispersion characteristics in liquid media. Our analysis revealed the synthesis of a spectrum of monodisperse bare and surface modified mesoporous silica nanoparticles with a narrow particle size distribution and devoid of cocontaminants critical for toxicity studies. Complete physicochemical characterization of these synthetic mesoporous silica nanoparticles will permit systematic toxicology studies for investigation of structure-activity relationships.

1. Introduction

Nanotechnology is an emerging field encompassing manufacture and use of materials with at least one dimension less than 100 nanometers [1]. The incorporation of engineered nanoparticles into household, personal care, consumer, and industrial products is increasing the exposure of humans and the ecosystems to these materials through production, transportation, storage, use, and disposal. Due to their small sizes, nanomaterials (NMs) can enter into cells and interact with cell organelles and/or macromolecules and may thus disrupt the normal cellular functions [1–4]. Various NMs have been observed to show systemic effects when administered into systemic circulation, either intentionally for biomedical therapy or accidentally during environmental exposures, and may even cross the blood/brain barrier [1, 3, 5].

SiO_2 is ubiquitous in our environment; human exposure can occur from natural or anthropogenic sources [6]. Advancement in nanotechnology in recent years has expanded the synthesis of nonporous silica nanoparticles

(SiNPs) for applications in catalytic supports [7], photonic crystals [8], and in biomedical fields including gene delivery, photodynamic therapy, and biomedical imaging [9–15]. The synthesis protocols can be easily optimized to produce monodisperse SiO_2 particles of selected sizes (mostly in ultrafine and micron range) and shapes. Meanwhile, the integration of surfactant templating methods with existing synthetic protocols of nonporous SiNPs can produce materials with different nanoscale sizes and enhanced porosity [16–20]. Furthermore, these protocols can be engineered to tune the pore sizes according to the requirements of specific applications, thus producing SiNPs with the desired structure, such as high surface area, large pore volume, and tunable pore structure and surface [16–20]. In addition, the surface of these SiNPs can then be easily functionalized [21]. Porous SiNPs contribute to versatility and contrast in various imaging modalities and are useful as drug/gene carriers in which the porous structures can be utilized to encapsulate the chemical/biological moieties to be delivered to the target tissue site directly [9–11, 15, 22, 23]. Another major application of such materials includes corrosion protection in which corrosion inhibitors are loaded into the mesopores [16]. The major advantage of these porous SiNPs is that they can be used as multifunctional platforms by integrating therapeutics and diagnostic functions in a single nanoparticle (NP) [22–24]. A successful multifunctional MS SiNP should exhibit the following characteristics: particle size uniformity, large pores with high pore volume, high colloidal stability in aqueous/biologically relevant media, optimized ability to be internalized by the target cells, good *in vitro*/*in vivo* traceability, the ability to perform triggered drug release, and degradation of the NPs after their designated function is accomplished, with minimum toxicological implications [23, 25].

Several facets of the synthesis including the design of the particle skeleton and surface modification of MS SiNPs must be considered carefully in order to maximize the benefits from their multifunctional nature. Previous studies have shown that the possible cellular internalization of SiNPs has been influenced by particle size with *ca.* 50 nm being the optimum size [26]. On the other hand, for applications as a drug carrier, a slightly larger NP with a higher pore volume and larger pore diameter is considered a better option. For effective drug loading or to obtain colloidal stability or traceability inside cells/tissues, the SiNP surface is generally first modified with chemical moieties such as alkylamine, alkylthiol, alkylcarboxy, fluorescein isothiocyanate, and rhodamine B isothiocyanate [27].

The objectives of this study were (1) to synthesize MS SiNPs with varying sizes, from a few nanometers to micron scale, with uniform particle size within each set, as well as with various surface functionalities and (2) to conduct complete physicochemical characterization of these materials in order to generate a library of reference materials for future toxicity studies. The synthesis of MS SiNPs over a wide particle size range entails several challenges. The first one is to devise a synthesis protocol using the same (or, with minimum changes in) starting chemicals to avoid the introduction of co-contaminants from different chemical species. The second challenge is to optimize overall yield of the synthesis, especially for particles below 60–70 nm, to generate appreciable amounts of materials in a single batch. The third challenge is to maintain the particle size uniformity as well as pore structure and pore size during the drying of powders and the surfactant removal process. It should be noted here that the general MS SiNP synthesis involves the micelle-templated protocols utilizing surfactants (and sometimes additional co-surfactants). The removal of surfactants, either using solvent extraction or calcining the as-synthesized materials at high temperature, is a critical step, as this can lead to undesirable structural changes, such as collapsed pore structures and/or disordered morphologies. The fourth challenge is to maintain the particle size and pore structure integrity during the postsynthesis surface modification process. Yamada et al. reported synthesis of MS SiNPs in a size range of 20 to 700 nm by utilizing tetra alkoxysilanes with different alkoxy groups as silica source and varying the type and amounts of co-surfactant alcohols (methanol, ethanol, propanol, and butanol) [19]. However, they observed relatively wide particle size distribution in each of those materials. In terms of toxicology studies of SiNPS, presence of co-contaminants and wider particle size distributions can introduce additional complexities. Another concern was the stability of pore structures of those materials during postsynthesis surface functionalization involving strong acid (H_2SO_4).

In this study, we report the synthesis and physicochemical characterization of a library of MS SiNPs in a wide range of particle sizes from low nanometer to micron range, and their corresponding different surface-modified forms. The study was designed to synthesize spherical MS SiNPs of five different sizes varying from 25 to 600 nm. Specific attention was given to synthesis of SiNPs with narrow particle size distributions and a minimum number of possible impurities coming from starting materials. Furthermore, two other sets of materials were synthesized by modifying the surface of all five materials with hydrophilic and relatively more hydrophobic functional groups that were relevant to intended toxicity studies.

2. Materials and Methods

2.1. Synthesis of Mesoporous Silica Nanoparticles

2.1.1. Synthesis of Mesoporous Silica Nanoparticles ca. 600 nm in Size (SiNP600). For the synthesis of mesoporous silica nanoparticles ca. 600 nm in size, 3.08 g of decyltrimethylammonium bromide (C10TMAB, Aldrich), and 4.56 mL of 1 M sodium hydroxide solution (Sigma-Aldrich, Oakville, ON, Canada) were dissolved in 800 mL of water. Then, 3.04 g of tetramethyl orthosilicate (TMOS, Aldrich) was added to the solution with vigorous stirring. After addition of TMOS, the clear solution gradually turned opaque finally resulting in a white precipitate. After 8 h of continuous stirring, the mixture was aged overnight. The white powder was then filtered out using 0.2 micron filter paper, washed with copious amounts of distilled water, and then dried at 318 K for 72 h. The powder obtained was calcined in air at 823 K for 6 h to remove any remaining organic species.

2.1.2. Synthesis of Mesoporous Silica Nanoparticles ca. 70, 100, and 170 nm in Size (SiNP70, SiNP100, and SiNP170, Resp.) In a typical synthesis of SiNP170, 32 mL of distilled water, 9 g of ethanol (Reagent Grade, Sigma-Aldrich, Oakville, ON, Canada), 5.2 g of a 25 wt% cetyltrimethylammonium chloride (CTAC, Sigma-Aldrich, Oakville, ON, Canada) solution, and 0.1 g of diethanolamine (DEA, Sigma-Aldrich, Oakville, ON, Canada) were mixed and stirred in a water bath at 60°C for 30 min. Then, 3.65 mL of tetraethyl orthosilicate (TEOS, Gelest, Morrisville, PA, USA) was added dropwise within 2 min under vigorous stirring. The solution gradually turned white during this addition. After 2 h of additional stirring, the mixture was cooled to room temperature: the precipitate was recovered by filtration using a 0.2 micron filter paper and washed thoroughly with distilled water. The material was dried at 318 K for 72 h and the silica nanoparticles obtained were calcined in air at 823 K for 6 h to remove any remaining organic species. SiNP70 was synthesized by following the same procedure as described above while varying the ethanol amount in the initial mixture (6.5 g instead of 9 g). Similarly, SiNP100 was synthesized by using 4.5 g of ethanol and 2.5 g of Na_2HPO_4–NaH_2PO_4 buffer solution (Sigma-Aldrich, Oakville, ON, Canada) instead of DEA.

2.1.3. Synthesis of Mesoporous Silica Nanoparticles ca. 25 nm in Size (SiNP25). In a typical synthesis, 0.29 g of cetyltrimethylammonium bromide (CTAB, Sigma-Aldrich, Oakville, ON, Canada) was dissolved in 150 mL of ammonium hydroxide solution (Sigma-Aldrich, Oakville, ON, Canada) at 333 K in a temperature controlled water bath. Then, 2.0 mL of 0.88 M ethanolic TEOS (Gelest, Morrisville, PA, USA) was added to the solution under vigorous stirring. After 1 h, the solution was aged at the same temperature for 18 h in static conditions. The as-synthesized colloid was filtered (0.2 micron filter paper) and washed with 50 mL of ethanolic ammonium nitrate solution (6 g/L, Sigma-Aldrich, Oakville, ON, Canada) twice for complete removal of CTAB. The sample was dried at 60°C overnight and calcined as described above.

2.2. Surface Modification of Mesoporous Silica Nanoparticles

2.2.1. Starting Materials for Surface Modifications. The yield of the silica nanoparticles during synthesis varied depending on their size and the yields from each batch are presented in Table 1. In order to obtain adequate amounts of materials for surface modifications with either hydrophilic (–CH_2–CH_2–CH_2–COOH) or relatively hydrophobic (–CH_2–(CH_2)10–COOH) functional groups, several batches of the same materials were synthesized. The size distributions of the nanoparticles (TEM/SEM) were measured to ascertain the reproducibility between batches. Then the batches of the same materials were combined to generate a pool, which was then divided into three parts. Two portions were used for surface modifications using hydrophilic and hydrophobic functional groups, respectively, whereas the third portion was kept unmodified.

2.2.2. Surface Modification with Carboxylic Acids. Incorporation of the organic functionality was achieved via surface grafting of 3-cyanopropyltriethyoxysilane (C_3CN) or 11-cyanoundecyltrimethyoxysilane ($C_{11}CN$) (Gelest, Morrisville, PA, USA), followed by acid hydrolysis using H_2SO_4 (Sigma-Aldrich, Oakville, ON, Canada) to their corresponding carboxylic acids. A specific amount of MS SiNPs was first dried in a vacuum oven at 120°C and then loaded into a multineck glass flask containing 10 mL of toluene per 100 mg of material. The contents of the flask were stirred until a homogeneous mixture was produced. Distilled deionized water at a ratio of 0.4 mL/g of silica was then added and the flask was left stirring for at least 30 min. The glass flask was fitted with a condenser and submerged in a silicon oil bath set at 85°C using a temperature controlled stirring hotplate with an external temperature probe. The appropriate organosilane (2 mL/g silica) was subsequently added to the mixture and left stirring for 16 h. Then, the material was filtered (0.22 micron filter paper) and washed with copious amounts of toluene followed by acetone. The recovered solid was dried and treated in 48 wt% aqueous sulfuric acid (170 mL/g of material) overnight at 95°C. The solid was recovered by filtration (0.22 micron filter paper), washed thoroughly with water and acetone, and then dried at room temperature overnight.

2.3. Physicochemical Characterizations of SiNPs

2.3.1. Imaging of Materials by Scanning and Transmission Electron Microscopy. Scanning and transmission electron microscopy (SEM and TEM) images were recorded to determine the average particle size and the morphology of the materials. A JSM-7500F FESEM instrument (JEOL, Peabody, MA, USA) was used for SEM analysis of all SiNPs except SiNP25. For TEM imaging of SiNP25, the sample was dispersed in ethanol using an ultrasonic bath, and a drop of the slurry was deposited on a carbon-coated copper grid and then dried in air. The images were recorded using a JEM-2100F FETEM (JEOL, Munich, Germany) instrument operated at beam strength of 200 kV. For both types of measurement, the average particle size was determined from the mean size of at least 50 individual particles using ImageJ 1.47 software.

2.3.2. Fourier Transformed Infrared Spectroscopy. Fourier transformed infrared (FTIR) analysis of all MS SiNPs was performed on a Nicolet 6700 FTIR spectrometer (Thermo Scientific, Waltham, USA) using KBr pellets following the method reported by Das et al. [28].

2.3.3. Analysis of BET Surface Area, Pore Volume, and Pore Size Distribution. All SiNPs were characterized by nitrogen adsorption at 77 K to measure their structural properties using an ASAP 2020 Physisorption Analyzer (Micromeritics, Norcross, GA, USA). Before adsorption measurements, all silica samples were degassed under vacuum (1×10^{-5} Torr) at 150°C for 3 h. Organically modified materials were outgassed at 100°C. The BET surface areas were calculated from the adsorption isotherm in the relative pressure range from 0.06

to 0.2. The pore size distributions (PSD) were calculated from the nitrogen adsorption data using the Barrett-Joyner-Halenda (BJH) method with Kruk-Jaroniec-Sayari (KJS) correction, and the peak maximum value of the PSD was reported as the average pore size. The pore volume was reported as the volume of liquid nitrogen adsorbed at P/P_0 = *ca.* 1.

2.3.4. Thermogravimetric Analysis. The organic content was determined by thermogravimetric analysis (TGA) using a TA Q-500 (TA Instruments). The sample was heated at 10°C/min under flowing nitrogen up to 800°C, followed by decomposition in the presence of air at the same heating rate from 800°C to 1000°C. The weight loss below 200°C was attributed to loss of adsorbed water, solvent, and any alcohol associated with the nonhydrolyzed alkoxy groups, if any. The organic content was calculated based on the weight loss beyond 200°C. Surface densities of the carboxylic groups were calculated with respect to the surface area of the unmodified SiNPs relative to their respective size group using the following formula:

$$\mathrm{SD} = \frac{\mathrm{OC/MW\,(OS)}}{\mathrm{SA}\,(p)} \times 10^6, \quad (1)$$

where SD is the surface density of the organic groups (μmol/m^2), OC is the organic content (moles) per gram of SiNP, MW(OS) is the molecular weight of the organic substrate, and SA(p) is the surface area (m^2/g) of unmodified SiNP.

2.3.5. Particle Size Measurement in Liquid Media by Dynamic Light Scattering. The hydrodynamic diameter of the synthesized and functionalized SiNPs was determined by dynamic light scattering (DLS) measurements. Nanoparticles were suspended in double distilled water at 1 mg/mL concentration, vortexed for 10 s, and sonicated for 15 min. After sonication, the SiNPs were diluted to 0.15 mg/mL and again sonicated for 15 min, followed by size measurements using a Zetasizer Nano ZS (Malvern Instruments, UK) employing a nominal 5 mW HeNe laser operating at a 633 nm wavelength; the scattered light was detected at 173°. The refractive index (1.33) and the viscosity (0.89) of ultrapure water at 25°C were used in the data analysis performed in automatic mode using the instrument software (DTS 6.0). All measurements were performed in duplicate in three independent experiments with each of the duplicates measured 15 times to obtain an average particle size measurement. The particle size reported as hydrodynamic diameter was obtained from the intensity distribution by cumulant analysis. These nanoparticles were further subjected to zeta potential measurements on the same instrument by employing disposable zeta cells where laser Doppler velocimetry was used to calculate the zeta potential from the electrophoretic mobility. Zeta potential measurements were also carried out in duplicate in three independent experiments in automatic mode with the average of 15 measurements used for each sample within the duplicates.

Table 1: Yield of SiNPs during the synthesis process.

Sample name	Yield per batch (%)
SiNP25	<40
SiNP70	80
SiNP100	48
SiNP170	78
SiNP600	85

3. Results and Discussions

In this study, five mesoporous SiNPs with approximate unit particle sizes of 25 nm (SiNP25), 70 nm (SiNP70), 100 nm (SiNP100), 170 nm (SiNP170), and 600 nm (SiNP600) were synthesized using the surfactant template methods as described above. All SiNPs were prepared from the same source of silica (TEOS), except SiNP600 (in which TMOS was used), and by varying the amount of the same co-surfactant ethanol. However, as described in the experimental section (Section 2.1.2), Na_2HPO_4–NaH_2PO_4, buffer solution was used instead of DEA in order to synthesize SiNP100. In a recent report, Yamada et al. synthesized MS SiNPs in a size range of 20 to 700 nm utilizing a micelle-templated protocol by varying the silica source (tetra alkoxysilane with different alkoxy group) and the type and amounts of co-surfactant alcohols (methanol, ethanol, propanol, and butanol) [19]. The authors adopted dialysis as the surfactant removal process rather than calcination (which may result in collapsed pores) in order to retain pore structure integrity and high dispersibility of MS SiNPs in water. The utilization of silanes with different alkoxy groups as silica source and alcohol types as co-surfactants may produce materials with different alcohol impurities retained inside the material structures, which, in turn, could influence the toxicological studies downstream. This is especially true because Yamada et al. adapted dialysis for removing surfactant instead of high temperature calcination, which would have removed alcohols during heating. Another concern was the stability of pore structures for postsynthesis surface functionalization involving strong acid (H_2SO_4) at 95°C (see Section 2.2.2). Moreover, they obtained relatively wide particle size distributions [19]. In our case, the surfaces of all MS SiNPs were modified with hydrophilic C_3–COOH and relatively hydrophobic C_{11}–COOH surface groups to produce materials named as SiNPXC_3 or SiNPXC_{11}, respectively, where X is the corresponding mean particle diameter (e.g., X = 25, 70, 100, 170, and 600). The surface-modified SiNPs were included in the list of materials to be synthesized since it is known that these functionalities can modify nano-particle-cell interactions. There are reports on the impact of surface modifications on cellular uptake mechanisms, reactive oxygen species formation, and inflammatory response [23, 29–31].

The physicochemical properties of all SiNPs, including the two surface modified forms, were analyzed using various techniques. The TEM or SEM images of SiNPs in their dry form exhibited unmodified SiNPs to be nearly monodisperse with spherical morphologies (Figures 1(a)–1(e)) and narrow

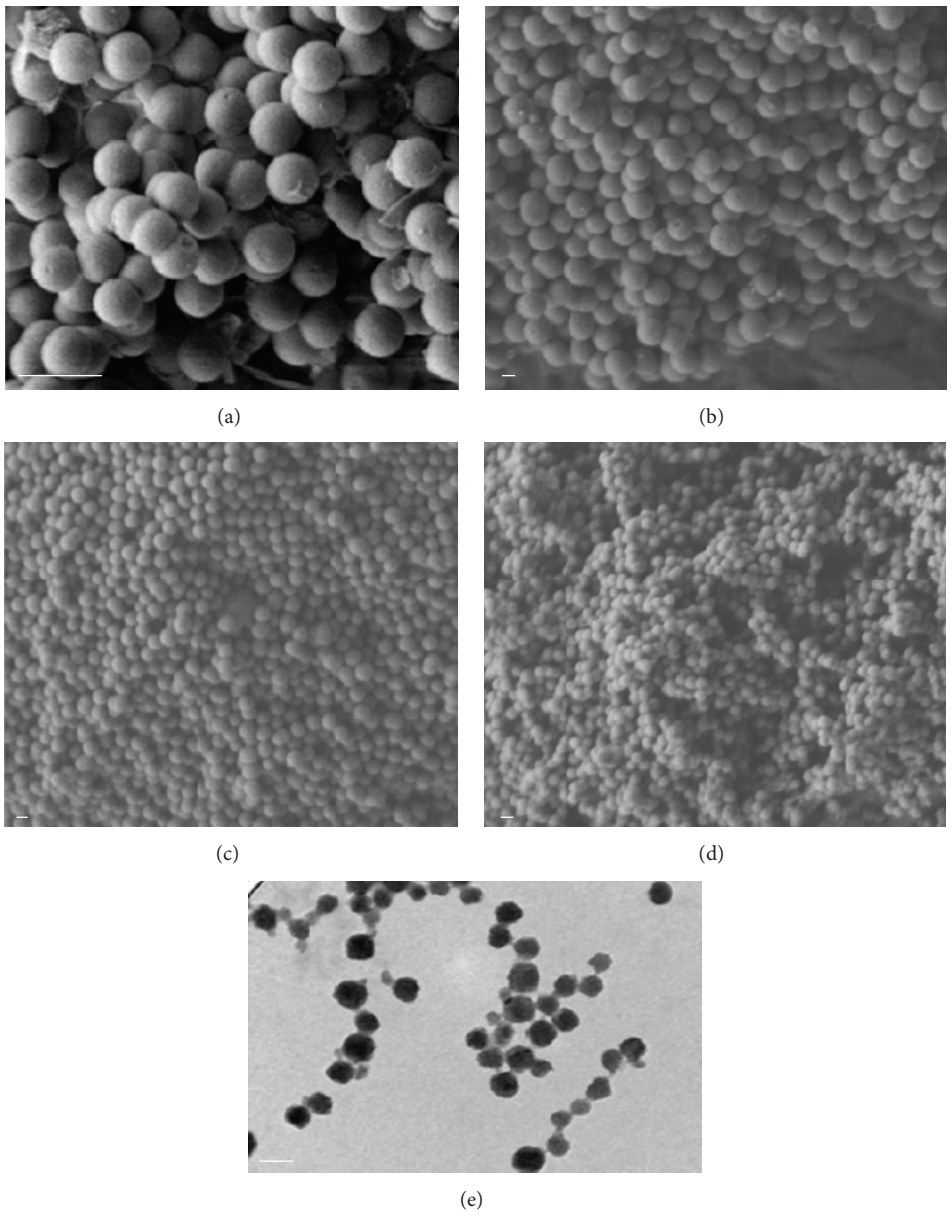

Figure 1: SEM images of SiNP600 (a, scale bar 1 μm); SiNP170 (b, scale bar 100 nm); SiNP100 (c, scale bar 100 nm); SiNP70 (d, scale bar 100 nm); and TEM image of SiNP25 (e, scale bar 50 nm).

particle size distribution (Table 2). Surface modifications of the SiNP600 with either C_3–COOH or C_{11}–COOH groups did not alter the size and morphology of the original pristine particles (Figure 2(a) versus Figures 2(b) and 2(c)). Similar results were obtained with all other nanoparticle sizes (data not shown).

The N_2 adsorption-desorption isotherms (Figure 3) for all unmodified SiNPs showed sharp steps typical of ordered mesoporous materials. The appearance of these steps at different relative pressures (P/P_0 in Figure 3) for different SiNPs was due to the capillary condensation/evaporation of nitrogen molecules inside the pores depending on the pore sizes of the material. All MS SiNPs were found to be highly porous with large surface areas and high pore volumes (Table 2). For instance, the BET analysis of SiNP25 exhibited a surface area of 1028 m^2/g and pore volume of 2.1 cm^3/g. Surface area and pore volume values associated with SiNP100 were 458 m^2/g and 0.5 cm^3/g, respectively, which were the lowest among all five unmodified SiNPs. The surface modifications of SiNPs of all sizes resulted in decreased surface areas and pore volumes compared to the corresponding unmodified SiNPs (Table 2), indicating partial blockage of pores due to the presence of organic functional groups on the surface. Similar observations of decreased surface area upon surface functionalization have been reported in the literature, in which various types of surface modifiers have been used

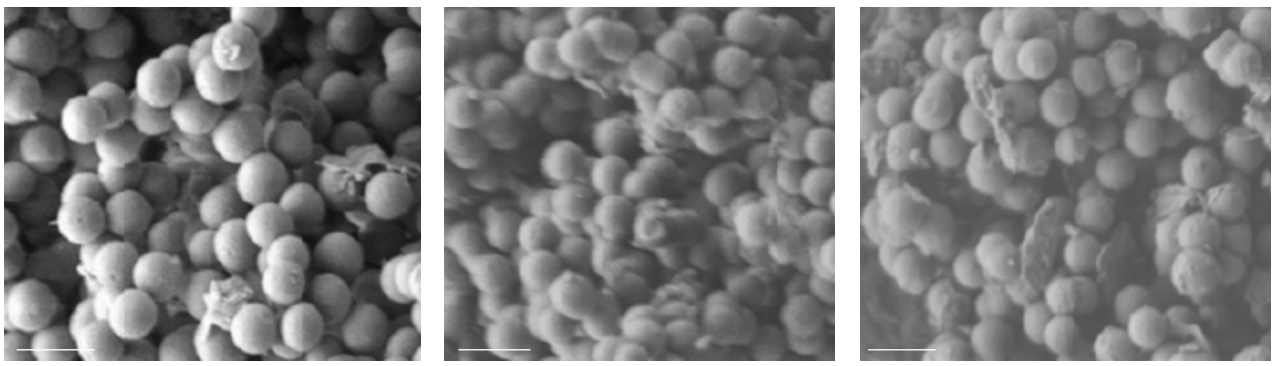

(a) (b) (c)

Figure 2: SEM images of SiNPs before and after surface modification: unmodified (a); C_3–COOH (b); and C_{11}–COOH modified SiNP600 (c). Scale bar is 1 μm in each case.

Table 2: Physicochemical and surface properties of both pristine and surface-modified SiNPs.

Sample name	Particle diameter* (nm)	Surface modifier	BET surface area (m^2/g)	Pore volume (cm^3/g)	Organic content# (wt%)	Surface density of –COOH (μmol/m^2)
SiNP25	27 ± 4.3	—	1028	2.1	—	—
		C_3–COOH	607	1.21	16.6	1.85
		C_{11}–COOH	495	1.05	22.0	1.16
SiNP70	67 ± 9	—	722	0.62	—	—
		C_3–COOH	456	0.35	10.6	1.69
		C_{11}–COOH	37§	0.17§	21.0	1.57
SiNP100	99 ± 10	—	458	0.50	—	—
		C_3–COOH	257	0.30	5.6	1.40
		C_{11}–COOH	183	0.15	10.4	1.23
SiNP170	177 ± 12	—	1011§	0.73§	—	—
		C_3–COOH	522§	0.48§	11.2	1.30
		C_{11}–COOH	185§	0.29§	12.2	0.61
SiNP600	596 ± 29	—	850§	0.51§	—	—
		C_3–COOH	342§	0.41§	11.5	1.59
		C_{11}–COOH	149§	0.25§	9.8	0.58

*Size determined from SEM/TEM analysis; #organic content was measured by TGA.
§BET surface area and pore volume are the average of results obtained from two different laboratories. The variance of the measurements was within 10%.

[32]. In general, C_{11}–COOH modified SiNPs showed lower surface areas and pore volumes relative to the C_3–COOH modified SiNPs (Table 2). This may be due to a higher degree of pore blockages due to the bulkier C_{11}–COOH groups.

The Fourier transformed infrared spectra (FTIR) of both C_3–CN and C_{11}–CN modified SiNP100C_3–CN showed a peak at 2247 cm^{-1} (Figure 4), which was assigned to the stretching vibration of C≡N group. The same peak was also observed for SiNP100C_{11}-CN (data not shown). Upon acid hydrolysis, this peak disappeared and a new peak was observed at 1713 cm^{-1} for all of the carboxyl functionalized materials (Figure 4), which was assigned to the C=O stretching vibration in the carboxylic group. FTIR spectrum of a mixture of silica and malonic acid (2nd spectrum from top in Figure 4) showed the same peak further confirming the presence of C=O stretching vibration. These results provide evidence to support the successful incorporation of C≡N groups on the SiNP surface and their subsequent oxidation to –COOH groups using the acid hydrolysis process. Similar spectra were obtained for the other SiNPs (data not shown), indicating the successful surface modifications of those nanoparticles. It should be noted here that the acid hydrolysis is a harsh process involving the strong mineral acid H_2SO_4, which can potentially have an impact on the structural properties of the silica matrices [33]. However, our results from the SEM images (Figures 2(a)–2(c)) indicated that no such changes occurred in the morphology of any of the surface-modified SiNPs in this study.

Figure 5 depicts the thermogravimetric analysis (TGA) of the surface-modified SiNPs functionalized with carboxyl groups. The weight loss below 200°C was attributed to the removal of physically adsorbed water and any remaining

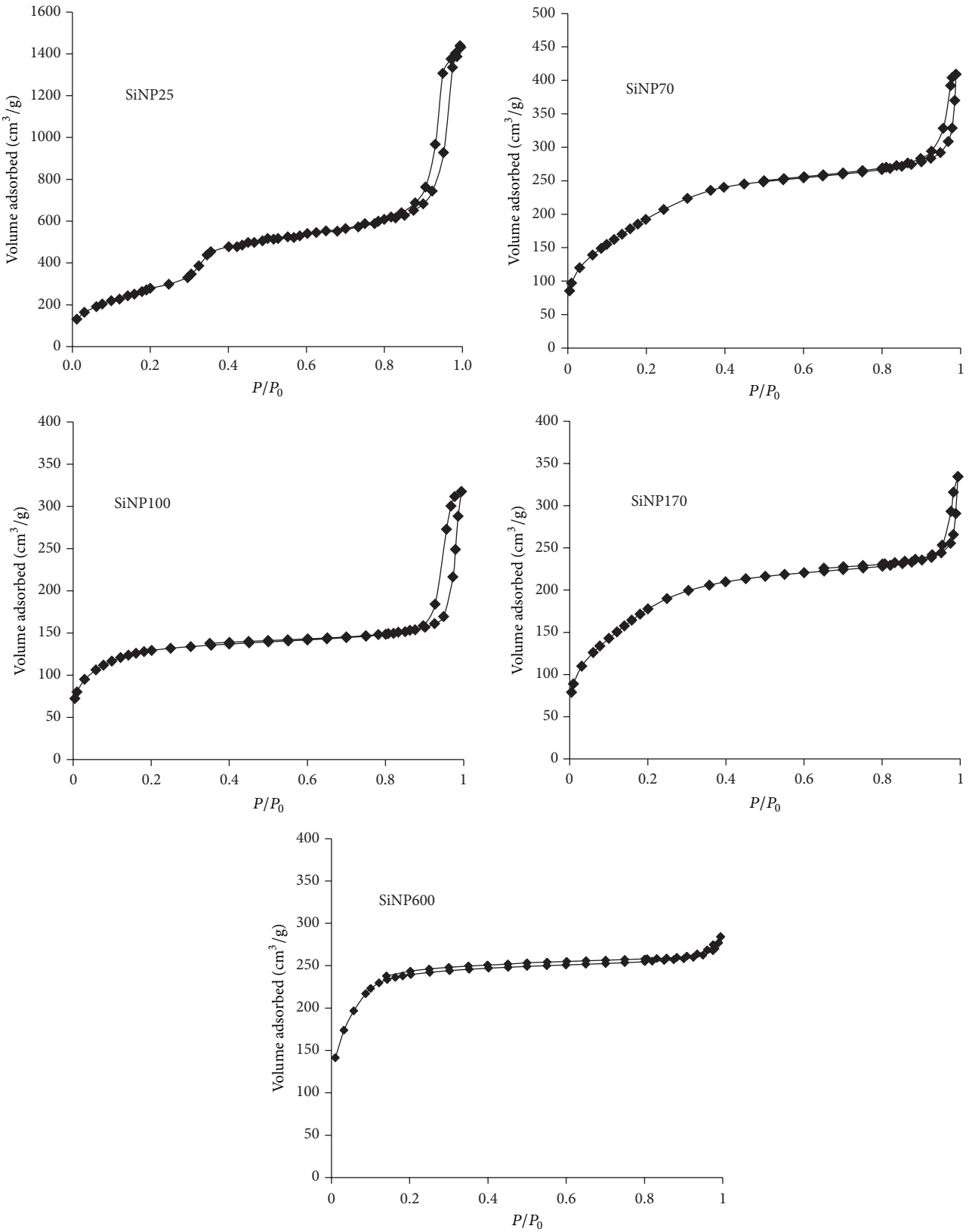

Figure 3: Nitrogen adsorption/desorption isotherms of unmodified SiNPs.

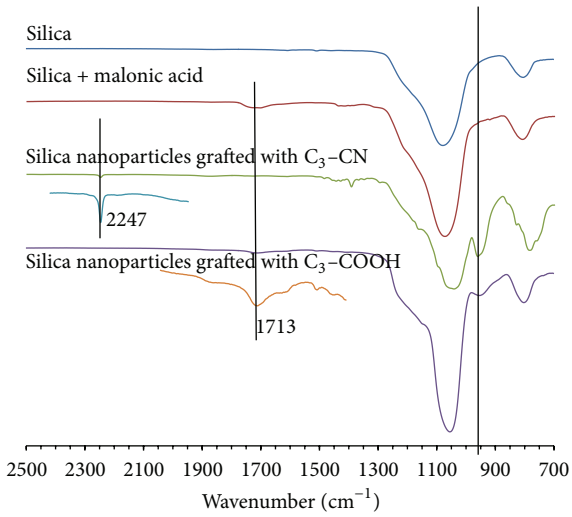

Figure 4: Fourier transformed infrared (FTIR) spectra of SiNP100 along with the C_3–CN and C_3–COOH surface modified materials. The spectra are expanded in Y-axis in the regions to show the stretching vibrations of C≡N at 2247 cm^{-1} and C=O at 1713 cm^{-1} for C_3–CN and C_3–COOH surface modified materials, respectively. Malonic acid adsorbed on silica surface is used as an internal reference.

Table 3: Particle size and zeta potential of SiNPs as measured by dynamic light scattering (DLS) in deionized water at pH 6.5 (SiNP concentration 150 μg/mL).

Particles	DLS size ± SD (nm)	PDI	Zeta potential ± SD (mV)
SiNP25	406 ± 147	0.49	−27.1 ± 0.9
SiNP25C3	386 ± 51	0.41	−28.6 ± 1.3
SiNP25C11	330 ± 49	0.41	−32.8 ± 2.2
SiNP70	253 ± 61	0.4	−22.3 ± 2.5
SiNP70C3	219 ± 17	0.25	−30.3 ± 4.1
SiNP70C11	217 ± 28	0.3	−31.8 ± 0.8
SiNP100	191 ± 23	0.23	−37.6 ± 6.4
SiNP100C3	185 ± 15	0.17	−43.5 ± 2.1
SiNP100C11	190 ± 6	0.17	−39.5 ± 5.8
SiNP170	266 ± 13	0.28	−38.2 ± 1.1
SiNP170C3	319 ± 36	0.34	−45.8 ± 1.1
SiNP170C11	213 ± 10	0.18	−44.0 ± 1.3
SiNP600	709 ± 76	0.4	−40.1 ± 1.7
SiNP600C3	768 ± 126	0.38	−48.0 ± 0.7
SiNP600C11	612 ± 65	0.4	−43.6 ± 1.4

solvent molecules from the synthesis and functionalization processes, as well as nonhydrolysed alkoxy groups from the SiNP surface. There was a gradual weight loss in the temperature range of 200 to 600°C, which could be attributed to the loss of organic groups under the nitrogen atmosphere. There was a sudden weight loss near 800°C, likely due to the combustion of the surface organic functional groups under an air atmosphere. The weight loss between 200 and 1000°C was utilized in the calculation of the surface density of carboxylic groups on the functionalized SiNPs, the results of which are presented in Table 2. As can be observed from Column 7of Table 2, the surface density of the C_{11}–COOH groups was lower than that of C_3–COOH, irrespective of the size of the SiNPs. This could be attributed to the bulkier C_{11}–COOH organic groups leading to a less efficient grafting process than C_3–COOH.

Biomedical application of SiNPs is influenced by the interactions of the NPs with the lipid bilayers and cells in tissues. Moreover, the interactions of SiNPs with the constituents of the media used as a vehicle to administer the SiNPs can also potentially influence their interactions with the biological tissues/cells. These interactions are almost entirely dictated by the surface properties of SiNPs. Thus, it is important to characterize the surface properties of the SiNPs both in their dry state and also dispersed in the liquid phase.

SiNPs, like any other NMs, tend to form agglomerate/aggregates when dispersed in water or any other liquid media [34, 35]. In order to measure the degree of agglomeration/aggregation of the SiNPs in the aqueous phase and the influence of surface C_3–COOH and C_{11}–COOH groups on these properties, particle sizes of pristine and surface-modified SiNPs were measured using the dynamic light scattering (DLS) technique. Our results revealed that all SiNPs were dispersed up to the concentration of 300 μg/mL with no sign of particle settling when allowed to stand for 6 h. In order to avoid any settling of particles during the particle size and zeta potential measurements, a concentration of 150 μg/mL was selected for all fifteen variants of the SiNPs. Particle size measurement by DLS revealed that stable particle dispersions remained in water up to 48 hours at room temperature (Figure 6). The polydispersity index (PDI) values (Table 3) in DLS measurement for all SiNPs were below 0.5, further indicating that the dispersions were stable. As can be observed from Table 3, the smaller SiNPs were associated with larger hydrodynamic diameters relative to their dry state unit particle size measurements by SEM/TEM. For instance, SiNP25 exhibited the largest increase in hydrodynamic diameter. This can be attributed to a relatively higher tendency of smaller nanosized particles to form agglomeration/aggregation [36]. Furthermore, the surface-modified forms of smaller SiNPs (e.g., SiNP25 and SiNP70) showed smaller hydrodynamic diameters relative to their corresponding unmodified pristine counterparts, which can be due to increasing hydrophobic nature of the surface organic moiety (Table 3) preventing their agglomeration. The surface modifications in the other three larger sized SiNPs (i.e., SiNP100, SiNP170, and SiNP600) did not show any appreciable changes in hydrodynamic diameters (Table 3). Negative zeta potentials were observed for all SiNPs and the values varied between −27 and −48 mV, except for SiNP70 (−22 mV) (Table 3). These results revealed stable SiNP dispersions in water with negatively charged surfaces. In the surface-modified SiNPs, the organic groups can act as surface stabilizers. This can be further supported by the low negative zeta potential for smaller sized SiNPs (nearly at −30 mV) and associated relatively larger hydrodynamic diameter for charge stabilization (Table 3). Since, it is known that the solids with

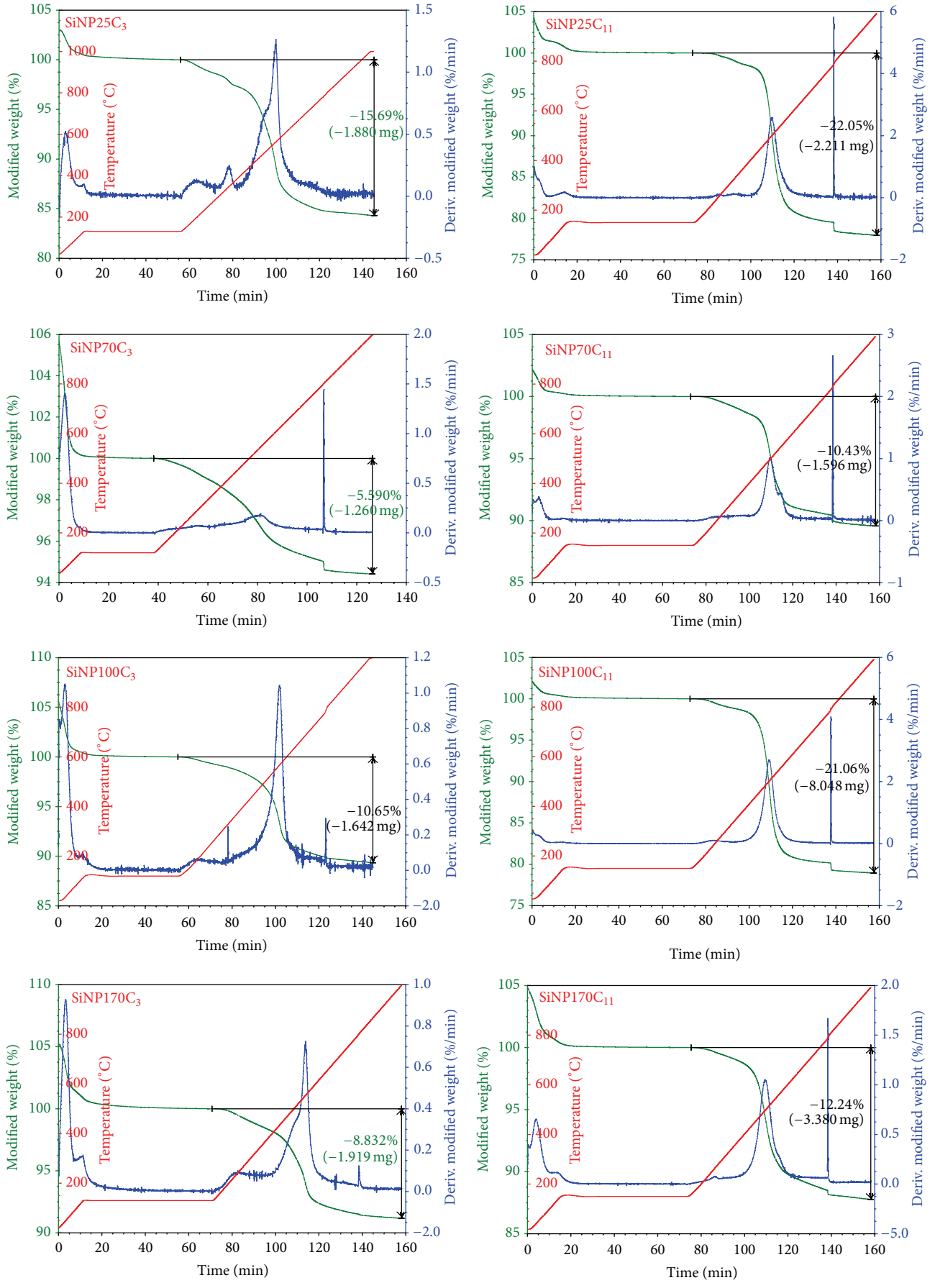

(a)

Figure 5: Continued.

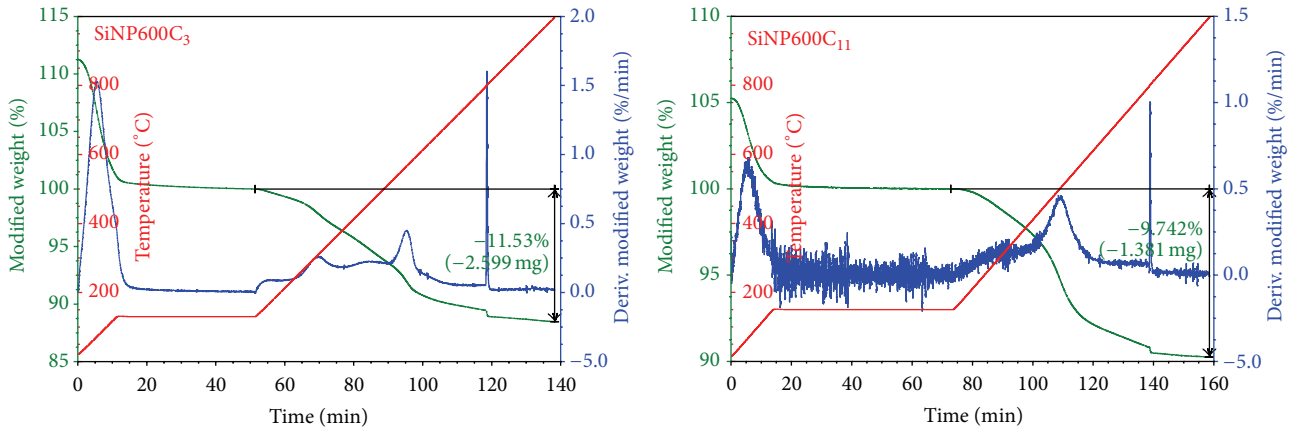

(b)

Figure 5: Thermogravimetric analysis (TGA) of surface modified SiNPs.

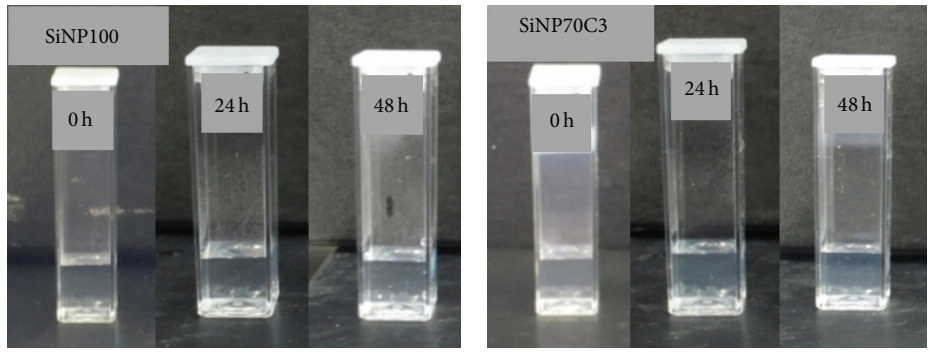

(a) (b)

Figure 6: Dispersion of two selected SiNPs in water at a concentration of 150 μg/mL.

stable surfaces produce zeta potential values between −30 and −50 mV in deionized water at neutral pH [37], the borderline values of *ca.* −30 mV observed for smaller sized SiNPs, irrespective of the presence or absence of surface modification, indicate that the surfaces of the smaller particles are relatively less stable than those of the larger SiNPs in water dispersions. The agglomeration/aggregation state, expressed as the ratio of the DLS size to the mean dry particle size measured by TEM/SEM for all SiNPs, is illustrated by Figure 7. Overall, larger aggregates/agglomerates were observed for smaller sized SiNPs. The hydrodynamic diameter for SiNP25 was ~16 times that of its mean dry particle diameter measured by TEM. It is well known that the hydrodynamic diameters are always larger than unit particle sizes measured in dry state. For example, Lu et al. [36] observed an increase in size of ~5 times in water for MS SiNPs of ~30 nm. However, it should be noted that the authors used solvent extraction for the removal of surfactants. The higher size ratio in our case could be due to the use of calcination procedure for the removal of surfactant, which may influence particle aggregation/agglomeration [36]. It should be noted that the TEM analysis (Figure 1(e)) in our case does not show aggregation of these particles. We observed higher difference for SiNP25 in aqueous suspensions, which could, therefore, be attributed to agglomeration of hydrated particles. Meanwhile, the SiNP70 particles appear to exhibit moderate agglomeration (4 times of mean dry particle diameter) and SiNPs of particle sizes ≥100 nm do not show much agglomeration. For instance, the TEM and DLS size of SiNP600 are almost identical within the analytical variability of the latter measurement. We also observed the impact of surface functionality on the DLS sizes of SiNPs ≤70 nm, implying that the surface groups may be assisting in dispersion. As opposed to particle aggregations, agglomerated particles are held together by weak attractive forces. These agglomerates can thus easily dissociate in the presence of small amounts of surfactants that are typically encountered in toxicological exposures. Thus these particles are useful for the purpose of toxicological studies as envisioned by the authors.

4. Conclusions

Five unmodified mesoporous silica nanoparticles (SiNPs) in the size range of *ca.* 25 nm to 600 nm were successfully synthesized. The synthesis conditions were optimized such that

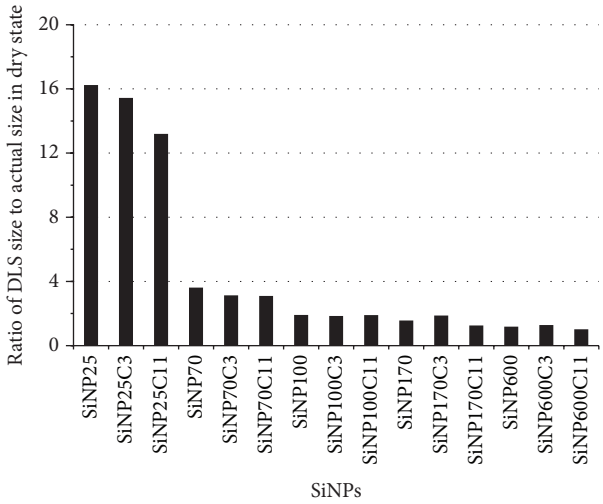

Figure 7: The ratio of agglomerated/aggregated particle size in water (measured by DLS) to the dry state particle size (measured by SEM/TEM) of unmodified and surface modified SiNPs.

SiNPs of different sizes are produced with monodispersed spherical morphologies, yet devoid of co-contaminants originating from sources. C_3–COOH and C_{11}–COOH groups were grafted onto the surfaces of the corresponding pristine SiNPs to produce hydrophilic and relatively more hydrophobic surfaces. Physicochemical characteristics of all 15 pristine and surface-modified SiNPs were analysed to determine the surface area, porosity, particle size distribution in the dry state and in aqueous dispersion, surface functionality, and surface charge. Establishment of this library of well characterized mesoporous SiNPs will enable the systematic analysis of toxicity of unmodified and surface-modified SiNPs for estimation of risk associated with such nanomaterials.

Conflict of Interests

The authors declare that there is no conflict of interests regarding the publication of this paper.

Acknowledgments

The authors thank Abdul Afghan and Lie Chen (Nanotechnology Section, New Substances Assessment and Control Bureau, Healthy Environments and Consumer Safety Branch, Health Canada) for comments and suggestions during the planning stages of this work. The funding from CMP Nano Initiative and New Substances Assessment and Control Bureau of Health Canada is greatly acknowledged.

References

[1] A. Nel, T. Xia, L. Mädler, and N. Li, "Toxic potential of materials at the nanolevel," *Science*, vol. 311, no. 5761, pp. 622–627, 2006.

[2] K. Donaldson, V. Stone, A. Clouter, L. Renwick, and W. MacNee, "Ultrafine particles," *Occupational and Environmental Medicine*, vol. 58, no. 3, pp. 211–216, 2001.

[3] G. Oberdörster, E. Oberdörster, and J. Oberdörster, "Nanotoxicology: an emerging discipline evolving from studies of ultrafine particles," *Environmental Health Perspectives*, vol. 113, no. 7, pp. 823–839, 2005.

[4] R. F. Service, "Nanotechnology grows up," *Science*, vol. 304, no. 5678, pp. 1732–1734, 2004.

[5] P. J. A. Borm and W. Kreyling, "Toxicological hazards of inhaled nanoparticles—potential implications for drug delivery," *Journal of Nanoscience and Nanotechnology*, vol. 4, no. 5, pp. 521–531, 2004.

[6] T. K. Barik, B. Sahu, and V. Swain, "Nanosilica—from medicine to pest control," *Parasitology Research*, vol. 103, no. 2, pp. 253–258, 2008.

[7] J. Kim, J. E. Lee, J. Lee et al., "Generalized fabrication of multifunctional nanoparticle assemblies on silica spheres," *Angewandte Chemie—International Edition*, vol. 45, no. 29, pp. 4789–4793, 2006.

[8] Y. S. Lin, Y. Hung, H. Y. Lin, Y. H. Tseng, Y. F. Chen, and C. Y. Mou, "Photonic crystals from monodisperse lanthanide-hydroxide-at-silica core/shell colloidal spheres," *Advanced Materials*, vol. 19, no. 4, pp. 577–580, 2007.

[9] S. Gandhi, K. Thandavan, B. J. Kwon et al., "Mesoporous silica: a highly promising and compatible candidate for optical and biomedical applications," *RSC Advances*, vol. 4, no. 12, pp. 5953–5962, 2014.

[10] Q. He and J. Shi, "Mesoporous silica nanoparticle based nano drug delivery systems: synthesis, controlled drug release and delivery, pharmacokinetics and biocompatibility," *Journal of Materials Chemistry*, vol. 21, no. 16, pp. 5845–5855, 2011.

[11] Z. Li, J. C. Barnes, A. Bosoy, J. F. Stoddart, and J. I. Zink, "Mesoporous silica nanoparticles in biomedical applications," *Chemical Society Reviews*, vol. 41, no. 7, pp. 2590–2605, 2012.

[12] C. W. Lu, Y. Hung, J. K. Hsiao et al., "Bifunctional magnetic silica nanoparticles for highly efficient human stem cell labeling," *Nano Letters*, vol. 7, no. 1, pp. 149–154, 2007.

[13] T. Y. Ohulchanskyy, I. Roy, L. N. Goswami et al., "Organically modified silica nanoparticles with covalently incorporated photosensitizer for photodynamic therapy of cancer," *Nano Letters*, vol. 7, no. 9, pp. 2835–2842, 2007.

[14] I. Roy, T. Y. Ohulchanskyy, D. J. Bharali et al., "Optical tracking of organically modified silica nanoparticles as DNA carriers: a nonviral, nanomedicine approach for gene delivery," *Proceedings of the National Academy of Sciences of the United States of America*, vol. 102, no. 2, pp. 279–284, 2005.

[15] F. Tang, L. Li, and D. Chen, "Mesoporous silica nanoparticles: synthesis, biocompatibility and drug delivery," *Advanced Materials*, vol. 24, no. 12, pp. 1504–1534, 2012.

[16] D. Borisova, H. Möhwald, and D. G. Shchukin, "Mesoporous silica nanoparticles for active corrosion protection," *ACS Nano*, vol. 5, no. 3, pp. 1939–1946, 2011.

[17] L. Han, Y. Zhou, T. He et al., "One-pot morphology-controlled synthesis of various shaped mesoporous silica nanoparticles," *Journal of Materials Science*, vol. 48, no. 17, pp. 5718–5726, 2013.

[18] S. H. Wu, C. Y. Mou, and H. P. Lin, "Synthesis of mesoporous silica nanoparticles," *Chemical Society Reviews*, vol. 42, no. 9, pp. 3862–3875, 2013.

[19] H. Yamada, C. Urata, H. Ujiie, Y. Yamauchi, and K. Kuroda, "Preparation of aqueous colloidal mesostructured and mesoporous silica nanoparticles with controlled particle size in a very wide range from 20 nm to 700 nm," *Nanoscale*, vol. 5, no. 13, pp. 6145–6153, 2013.

[20] K. Zhang, L. L. Xu, J. G. Jiang et al., "Facile large-scale synthesis of monodisperse mesoporous silica nanospheres with tunable pore structure," *Journal of the American Chemical Society*, vol. 135, no. 7, pp. 2427–2430, 2013.

[21] P. Yang, S. Gai, and J. Lin, "Functionalized mesoporous silica materials for controlled drug delivery," *Chemical Society Reviews*, vol. 41, no. 9, pp. 3679–3698, 2012.

[22] S. P. Hudson, R. F. Padera, R. Langer, and D. S. Kohane, "The biocompatibility of mesoporous silicates," *Biomaterials*, vol. 29, no. 30, pp. 4045–4055, 2008.

[23] Y. S. Lin, K. R. Hurley, and C. L. Haynes, "Critical considerations in the biomedical use of mesoporous silica nanoparticles," *Journal of Physical Chemistry Letters*, vol. 3, no. 3, pp. 364–374, 2012.

[24] J. M. Rosenholm, C. Sahlgren, and M. Lindén, "Multifunctional mesoporous silica nanoparticles for combined therapeutic, diagnostic and targeted action in cancer treatment," *Current Drug Targets*, vol. 12, no. 8, pp. 1166–1186, 2011.

[25] Y. S. Lin, N. Abadeer, K. R. Hurley, and C. L. Haynes, "Ultrastable, redispersible, small, and highly organomodified mesoporous silica nanotherapeutics," *Journal of the American Chemical Society*, vol. 133, no. 50, pp. 20444–20457, 2011.

[26] W. K. Oh, S. Kim, M. Choi et al., "Cellular uptake, cytotoxicity, and innate immune response of silica-titania hollow nanoparticles based on size and surface functionality," *ACS Nano*, vol. 4, no. 9, pp. 5301–5313, 2010.

[27] D. Tarn, C. E. Ashley, M. Xue, E. C. Carnes, J. I. Zink, and C. J. Brinker, "Mesoporous silica nanoparticle nanocarriers: biofunctionality and biocompatibility," *Accounts of Chemical Research*, vol. 46, no. 3, pp. 792–801, 2013.

[28] D. D. Das, P. J. E. Harlick, and A. Sayari, "Applications of pore-expanded MCM-41 silica: 4. Synthesis of a highly active base catalyst," *Catalysis Communications*, vol. 8, no. 5, pp. 829–833, 2007.

[29] X. Huang, L. Li, T. Liu et al., "The shape effect of mesoporous silica nanoparticles on biodistribution, clearance, and biocompatibility in vivo," *ACS Nano*, vol. 5, no. 7, pp. 5390–5399, 2011.

[30] A. Malugin, H. Herd, and H. Ghandehari, "Differential toxicity of amorphous silica nanoparticles toward phagocytic and epithelial cells," *Journal of Nanoparticle Research*, vol. 13, no. 10, pp. 5381–5396, 2011.

[31] A. Verma and F. Stellacci, "Effect of surface properties on nanoparticle-cell interactions," *Small*, vol. 6, no. 1, pp. 12–21, 2010.

[32] Y. S. Lin, N. Abadeer, and C. L. Haynes, "Stability of small mesoporous silica nanoparticles in biological media," *Chemical Communications*, vol. 47, no. 1, pp. 532–534, 2011.

[33] K. F. Lam, K. L. Yeung, and G. Mckay, "Selective mesoporous adsorbents for $Cr_2O_7^{2-}$ and Cu^{2+} separation," *Microporous and Mesoporous Materials*, vol. 100, no. 1–3, pp. 191–201, 2007.

[34] L. K. Limbach, Y. Li, R. N. Grass et al., "Oxide nanoparticle uptake in human lung fibroblasts: effects of particle size, agglomeration, and diffusion at low concentrations," *Environmental Science and Technology*, vol. 39, no. 23, pp. 9370–9376, 2005.

[35] S. K. Sohaebuddin, P. T. Thevenot, D. Baker, J. W. Eaton, and L. Tang, "Nanomaterial cytotoxicity is composition, size, and cell type dependent," *Particle and Fibre Toxicology*, vol. 7, article 22, 2010.

[36] F. Lu, S. H. Wu, Y. Hung, and C. Y. Mou, "Size effect on cell uptake in well-suspended, uniform mesoporous silica nanoparticles," *Small*, vol. 5, no. 12, pp. 1408–1413, 2009.

[37] L. Vaisman, G. Marom, and H. G. Wagner, "Dispersions of surface-modified carbon nanotubes in water-soluble and water-insoluble polymers," *Advanced Functional Materials*, vol. 16, no. 3, pp. 357–363, 2006.